Article

Interplay of Electronic Structure and Atomic Mobility in Nanoalloys of Au and Pt
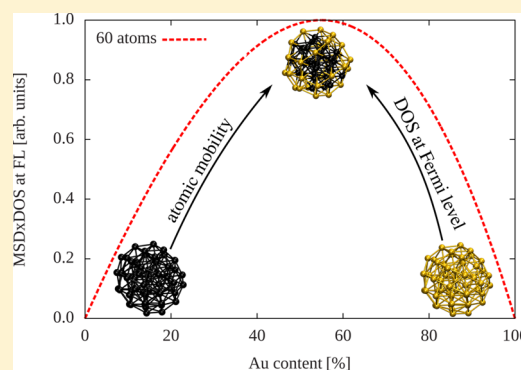
L. Leppert,[†] R. Q. Albuquerque,[‡] A. S. Foster,[§] and S. Kümmel*[,†]

[†]Theoretical Physics IV, University of Bayreuth, D-95440 Bayreuth, Germany
[‡]Institute of Chemistry of São Carlos, University of São Paulo, 13560-970 São Carlos-SP, Brazil
[§]COMP/Department of Applied Physics, Aalto University School of Science, P.O. Box 11100, FI-00076 Aalto, Finland

ABSTRACT: Nanoalloys of gold and platinum show special chemical qualities. As catalysts, for example, they are superior to pure Au and Pt nanoparticles under rather different experimental conditions. We demonstrate that combining Au and Pt leads to an advantageous combination of properties: The Pt component contributes a high density of states close to the Fermi level, which can promote chemical activity. The Au component increases the atomic mobility, which can allow the particles to structurally adapt to different chemical situations and adsorbates. Special catalytic properties of Au−Pt nanoparticles are thus expected based on general considerations, that is, inherent properties of the Au and Pt component, respectively.

1. INTRODUCTION

Clusters containing between a few and several thousands of atoms have attracted the interest of physicists and chemists for decades now. This tremendous attention can be ascribed to the special electronic and geometric nature of many clusters, manifesting in, for example, optical, magnetic, and catalytic properties that can differ considerably from the respective bulk system. A prime example is the catalytic activity of gold nanoparticles (NPs).[1] Its discovery was followed by a still ongoing quest for yet more catalytically active nanomaterials.[2−7]

One promising route to increase turnover rates, enhance the element-specific selectivity of catalysts, and hence tailor the catalytic activity is alloying of two (or more) elements.[8] Gold−platinum (Au−Pt) nanoalloys, for instance, have proved valuable in increasing the turnover rates in methanol fuel cells[9−15] as well as in many other oxidation reactions.[16−20] A comprehensive understanding of how this synergistic effect arises is complicated by the complex chemical environment in which many reactions take place. The presence of solvents, a matrix in which the nanoalloys are stabilized, and elevated temperatures renders understanding liquid-phase heterogeneous catalysis a challenge, which is quite different from the well-controlled gas-phase and surface conditions from which a lot has been learned in the past.

In this contribution we therefore do not focus on a mechanistic explanation of specific catalytic reactions but on a combination of intrinsic properties of Au−Pt NPs that cannot be found in the pure metals: The density of states (DOS) at the Fermi level increases with increasing Pt content, and the atomic mobility increases with increasing Au content. Both of these properties can beneficially influence the chemical reactivity

because the former is generally related to the strength of the interaction with adsorbates[21] and the latter can allow the NP to structurally adjust to reactants and, for example, form adsorption sites[22] or support surface corrugation effects.[23] The fact that Au−Pt NPs can combine two rather different, beneficial properties with a relative strength that is given by the ratio of Au and Pt can be expected to be part of the explanation for why these NPs exhibit special chemical properties in many reactions and under a broad range of environmental conditions.

2. THEORETICAL AND COMPUTATIONAL APPROACH

For calculating the DOS we relied on density functional theory (DFT) and used the nonempirical Perdew−Burke−Ernzerhof generalized gradient approximation (PBE GGA)[24] as implemented in the Turbomole program package;[25] for details of the computational approach see ref 26. For systems for which the relevant upper orbitals are localized on similar length scales the Kohn−Sham DOS qualitatively maps the true DOS.[27,28] This condition is fulfilled in the case of Au−Pt nanoalloys. We calculated the DOS using a basis set of triple-ζ quality after structural relaxation of 20-atom (see also ref 26), 38-atom homogeneously mixed truncated octahedral clusters, and 60-atom core−shell clusters with different Au/Pt ratios. Representative cluster structures are shown in the inset of Figure 3. We deliberately chose the truncated octahedral geometry because it represents a cut-out of the fcc lattice, and the experimentally observed larger Au−Pt nanoalloys are often

faceted and bulk-like.[17] The geometry of the 60-atom $Au_{30}Pt_{30}$ cluster was taken from ref 29.

To study self-diffusion and calculate energy barriers for single Au and Pt adatoms on Au and Pt surfaces we used the nudged elastic band method.[30] It allows the determination of the minimum energy path between a given initial and final state. If this minimum energy path goes through one or several maxima as a function of the reaction coordinate, then the largest of these barriers can be regarded as the rate-determining step of the reaction or diffusion, respectively. Calculations were carried out with the Vienna ab initio simulation package (VASP)[31] using the PBE GGA[24] and employing the projector-augmented wave (PAW) method to describe the electron-ion interaction.[32] The cutoff energy for the plane-wave basis set was set to 450 eV. Pure and doped Pt and Au fcc(111) surfaces were modeled by four-layer slabs containing 4 × 4 atoms in each layer and being separated by 20 Å of vacuum. The bottom two layers were held fixed at the Pt (Au) bulk equilibrium distance of 3.977 (4.174) Å, while the other layers were allowed to fully relax. We checked that our results were converged with respect to the total number of layers and the number of fixed layers at the bottom of the slab. The Brillouin zone integrations were performed using Monkhorst−Pack k-point meshes of 5 × 5 × 1 size. We considered a diffusion step from a fcc to a hcp hollow site for different combinations of surfaces and adatoms, as depicted in Figure 1. In all of the cases the diffusion barrier was
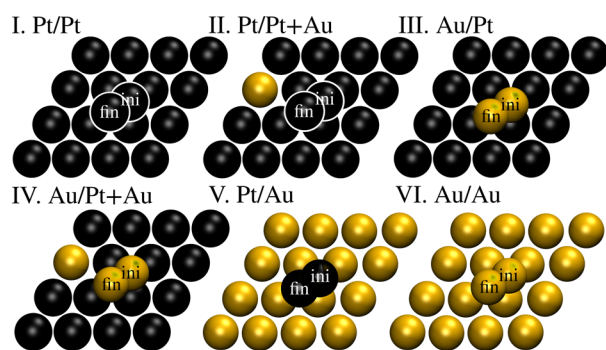
Figure 1. Sketch of the setup used for the study of Au and Pt adatom self-diffusion from a fcc (ini) to an hcp (fin) hollow position. The systems we studied were: (I) Pt adatom on pure Pt(111) surface, (II) Pt adatom on Pt(111) surface with single Au atom in top surface layer, (III) Au adatom on pure Pt(111) surface, (IV) Au adatom on Pt(111) doped with Au, (V) Pt adatom on Au(111), and (VI) Au adatom on Au(111).

defined as the energetic difference between the transition state and the hcp adsorption site, this being the largest energy difference and thus determining the rate of this particular diffusion step. In addition to the diffusion barriers we determined the adsorption energies (Table 1) of the adatoms at the fcc and hcp hollow site as

$$E_{ads} = E_{slab} + E_{adatom} - E_{slab+adatom} \quad (1)$$

The fluxionality of small Au clusters has recently been shown by extensive scans of their potential energy surfaces.[33] This method, however, is not feasible for Au−Pt nanoalloys in the experimentally relevant size range of ca. 3 to 4 nm (over a thousand atoms), and we also cannot employ DFT for these systems with many thousands of valence electrons. Therefore, we performed 1 ns long molecular dynamics (MD) simulations for randomly mixed truncated octahedral clusters with closed

Table 1. Adsorption Energies (in eV) of Pt and Au Adatoms in Pure and Doped Pt and Au Surfaces for the Start and the End Position of Each NEB Calculation[a]

system	E_{ads} fcc	E_{ads} hcp	$E_{barrier}$
Pt/Pt	4.60	4.82	312
Pt/Pt+Au	4.61	4.76	287
Au/Pt	2.77	2.87	177
Au/Pt+Au	2.79	2.86	165
Pt/Au	4.05	4.15	143
Au/Au	2.50	2.56	115

[a]For a definition of the diffusion barrier (in meV), see the text.

atomic shells of 38, 201, and 586 atoms, as illustrated in Figure 2 and for 60-atom and 100-atom core−shell clusters (from ref
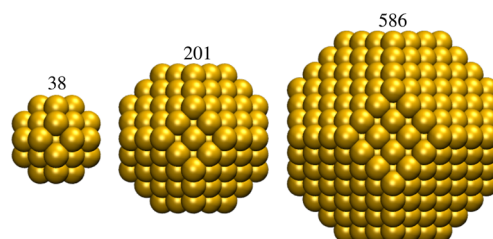
Figure 2. Truncated octahedral clusters with closed atomic shells of 38, 201, and 586 atoms. Au and Pt atoms (different ratios) were homogeneously distributed over the clusters to model Au−Pt solid solutions.

29) to obtain a measure of the mobility of the cluster atoms in terms of their mean-square displacement (MSD)

$$\langle \hat{r}^2 \rangle = \left\langle \frac{1}{N} \sum_{i=1}^{N} (\vec{r}_i(t) - \vec{r}_i(t=0))^2 \right\rangle \quad (2)$$

where N is the number of atoms in the cluster and $\vec{r}_i(t)$ is the position of atom i at time t. The angle brackets indicate a time average. The MD simulations were performed using the DL_POLY program[34] and the NVT Evans ensemble, which has been shown to describe Au−Pt NPs well.[35] The potential energy in the MD simulations was described by the well-tested[36−38] many-body Sutton−Chen (SC) potential.[39] Randomly mixed Au−Pt NPs segregate to $Au_{shell}Pt_{core}$ structures even at comparably modest temperatures and short simulation times. Because our aim was to retain the homogeneous mixing pattern of the truncated octahedra, all simulations were carried out at 300 K, with the exception of the 60-atom clusters for which MD simulations were carried out at a temperature of 200 K. These temperatures were chosen to ensure that in each case the temperature lies below the melting point of the system, in agreement with typical experimental conditions in which the NPs are also not molten. The use of low temperatures means that the MSD,[40,41] averaged over the whole (long) simulation time, is approximately zero. However, short-range motion can be observed at shorter time scales of 1000 fs. The time average in eq 2 was therefore computed for subsequent time windows of 1000 fs to extract information about this motion. For each Au/Pt mixing ratio three simulations were carried out to minimize statistical uncertainties. For NP in the size regime that we are concerned with the high surface-to-bulk ratio can have significant impact on the average MSD of the NP. Atoms at lowly coordinated positions, for example, at kinks or edges, can show MSDs that are considerably larger than those of highly

coordinated volume atoms or atoms in a surface plane. For irregular NPs like the 60-atom and the 100-atom NPs this effect is more pronounced than it is for the regular truncated octahedra with their magic atom numbers of 38, 210, and 586.

To obtain comparable MSD values it is therefore necessary to keep the geometries of NP with the same number of atoms but different Au/Pt ratios as close as possible. For the irregular 60-atom and 100-atom clusters this makes a full geometry optimization prior to MD simulations necessary. Nevertheless, the MSDs of these NPs show large statistical variations as compared with the MSDs of the truncated octahedra. For this reason we want to stress that we are not concerned with evaluating the exact value of the MSD in our NP but with the robust trend that the MSD shows with increasing Au content.

3. RESULTS AND DISCUSSION

The importance of the DOS for chemical properties is well known. In the context of catalysis, for example, the binding energy between adsorbates and metal surfaces can often be understood in terms of the d-band model.[42] It states, in its simplest form, that the closer the center of gravity of the metal d-band is relative to the Fermi level the stronger the adsorbate is bound to the surface. A shift of the d-band to higher energies is often accompanied by an increase in the total DOS at the Fermi level.[43] This is, in particular, true for the case of Au−Pt NPs. Figure 3 exemplifies this by comparing a pure Au_{38} to an $Au_{33}Pt_5$ cluster. As the center of the clusters' d-band (indicated

by the vertical blue line) moves closer to the Fermi level, the total DOS close to the Fermi level (integration threshold defined as −1 eV) increases. We verified this behavior for several cluster sizes and Au/Pt mixing ratios, and it has also been observed for other Pt-based nanoalloys.[44]

Figure 3b shows that the DOS at the Fermi level of Au−Pt NP increases as a function of the clusters' Pt content not only for the 20-atom clusters[26] but also for the larger 38-atom truncated octahedral clusters and 60-atom clusters. Two observations are important in Figure 3b: First, the increase in the DOS at the Fermi level with increasing Pt content is a very robust property with respect to both the cluster size and the geometric configuration of the clusters. Second, it is also independent of the specific mixing pattern: the 38-atom clusters have been constructed to show a homogeneous distribution of Au and Pt, whereas the 60-atom clusters are $Au_{shell}Pt_{core}$ clusters, and all show the characteristic dependence of the DOS on the Pt content.

The interaction between an NP and an adsorbate of course depends not only on the total DOS but also on local contributions to the electronic structure from different sites of the NP's surface.[45] In fact, active sites in the form of steps, kinks, and facets play a prominent role in the catalytic activity of Au surfaces.[22] It has been previously shown that the spatial location of the highest-occupied Kohn−Sham orbital (HOMO), which represents the spatial distribution of the energetically highest-lying part of the DOS, is always associated with the position of the Pt atoms.[26] Therefore, small structural surface rearrangements are followed by considerable changes of the local electronic structure. The "local electronic structure" perspective thus also supports the point of view that the presence of Pt in Au−Pt NPs should be beneficial to their reactivity on rather general grounds.

This finding can serve as a first hint for a synergistic effect, yet another property plays a role in Au−Pt NP: the mobility of the atoms in the Au−Pt system. Atomic mobility can be an indicator for the ability to structurally adjust to reactants and rebuild after the catalytic reaction. It has been recognized to be of crucial importance for the catalytic activity of clusters and surfaces.[46] To determine how easy it is for atoms to rearrange in Au−Pt systems, we performed two types of studies.

In the first one, we take the perspective that for the chemical and catalytic activity the surface of the NP, which for a faceted NP is similar to a bulk surface, is the most important part. When reactants approach the surface, structural rearrangements may take place that allow the formation of active sites for catalysis. The induction time[17,47,48] seen in NP catalysis can be an indication for such processes. A canonical step in such processes is the movement (diffusion) of atoms on the surface. Therefore, we determine the height of the barriers for the diffusion of Au and Pt adatoms on pure and doped Pt and Au surfaces. As an aside, we note that the surface point of view is also supported by the observation that bimetallic effects also play a role in Au−Pt surfaces.[49,50]

Figure 4a shows that diffusion of a Pt adatom on a pure Pt surface has the highest barrier of all considered systems. This is in line with the Pt adatom being most strongly adsorbed to the pure Pt surface, yet the insertion of one Au atom into the Pt surface lowers the diffusion barrier by ∼25 meV. A similar effect can be seen by comparing the diffusion barrier of an Au adatom on a pure Pt surface and on a Pt surface with one Au dopant. It is particularly interesting that the diffusion barrier decreases even more for a Pt adatom on a Au surface. In this case, the
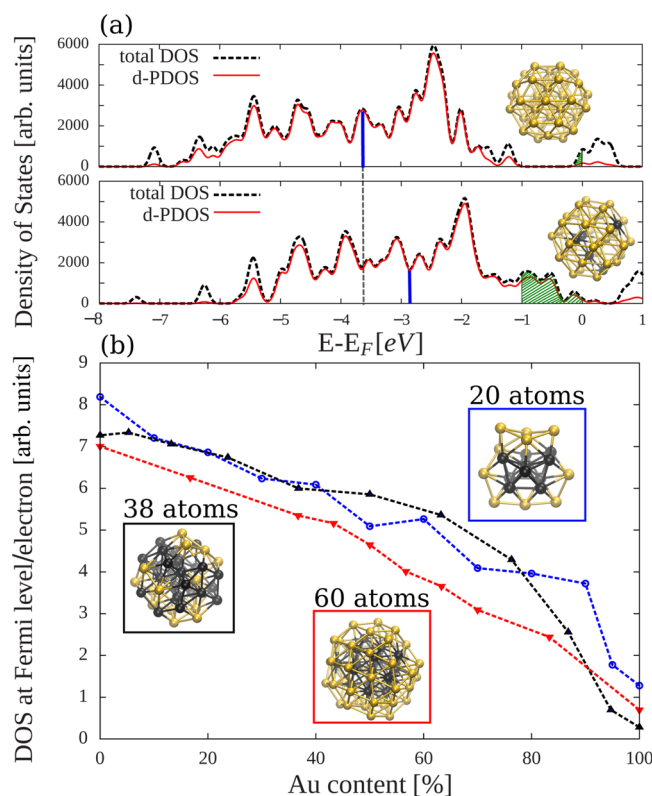

Figure 3. (a) Density of states and projected density of states for Au_{38} and $Au_{33}Pt_5$. The blue line indicates the center of gravity of the d-projected density of states, while the green shaded area shows the DOS within 1 eV below the Fermi level. (b) DOS at the Fermi level for 20-atom core−shell (blue circles), 38-atom randomly mixed (black circles), and 60-atom core−shell (red triangles) clusters decreases with increasing Au content of the clusters.
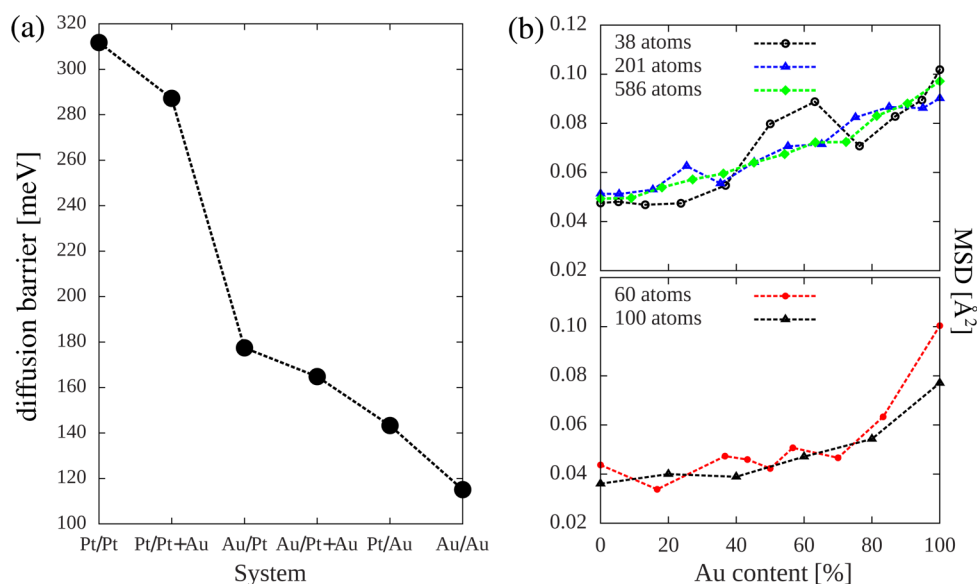
Figure 4. (a) Barrier for Pt- and Au-adatom diffusion on Pt surfaces with and without Au doping and on a pure Au surface. For explanation of the notation and the diffusion step, see Figure 1. (b) Top: MSDs from MD simulations of truncated octahedral clusters that are solid solutions of Au and Pt with 38 (black circles), 201 (green triangles), and 586 (blue diamonds) atoms. Bottom: MSDs of 60-atom (red circles) and 100-atom (black triangles) core−shell particles.

adsorption energy is almost as high as that of Pt on Pt(111), leading one to expect an equally high diffusion barrier. The facilitated surface diffusion on surfaces with a higher Au content can therefore not only be explained by Au adatoms being more weakly bound to the surface than Pt adatoms. We interpret this finding as an increased ability of Au-alloyed Pt surfaces to undergo structural changes.

In the second type of study that we did to show that increasing amounts of Au increase the atomic mobility in Au−Pt NPs, we moved away from the surface perspective and regarded the NPs as finite clusters. As explained in Section 2, we use the mean square displacement (MSD) of cluster atoms as a measure for atomic mobility. The MSDs are depicted in Figure 4b, showing the truncated octahedra in the upper and the 60-atom and 100-atom core−shell particles in the lower part of the Figure. It can clearly be seen that the composition-dependent trend is the same for all clusters: The MSD increases with increasing Au content. To put the magnitude of the increase that is seen in Figure 4b into perspective we note that an increase in the MSD by a factor of two would correspond to increasing the NP temperature by at least 100 K.[51] Figure 4b clearly shows that the trend of an increasing MSD with increasing Au content is again independent of particular geometric configurations or mixing patterns. Thus, although it is of a very different nature, the MD study confirms the conclusions drawn from the surface diffusion barrier calculations: structural flexibility increases with an increasing amount of Au.

In summary, we showed that the DOS of Au−Pt NP develops properties that one can associate with being favorable for reactivity and catalysis with increasing Pt content, whereas the structural flexibility increases with increasing Au content. Therefore, for different reactions and environments there can be an ideal ratio of Au and Pt that yields overall optimal properties. This is visualized in Figure 5. It shows the volcano-like plot that one obtains by multiplying the DOS at the Fermi level with the MSD (both shifted and smoothly interpolated as explained in the Appendix) for the 38-atom and 60-atom
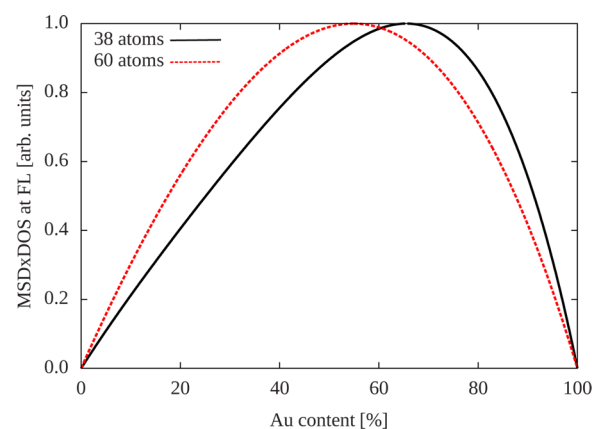

Figure 5. Product of the DOS at the Fermi level (FL) and the MSD for 38-atom and 60-atom Au−Pt clusters as a function of Au content. The DOS and MSD data were interpolated by polynomials. Quantities are shifted and scaled so that for 0 and 100% Au content the curves intersect the y axis at 0 and have a maximum value of 1. The "volcano" shape schematically visualizes that synergistic bimetallic effects can be expected on general grounds.

clusters. (For these systems we could access both quantities.) "Volcano plots" are often used to visualize Sabatier's principle, which states that there exists an optimal interaction strength between a catalyst and the reactants.[52] Of course, our observation here is rather general and cannot be used to predict the optimal mixing ratio for a specific reaction. The latter will sensitively depend on the reaction details, experimental conditions such as solvents, and the exact structure and mixing pattern of the catalysts, yet the point that Figure 5 emphasizes is that synergistic effects in Au−Pt NPs are expected on rather general grounds and regardless of the specific chemical reaction and environment. Our study thus contributes one step in the understanding of why Au−Pt NPs can show useful properties under many different chemical and physical conditions.
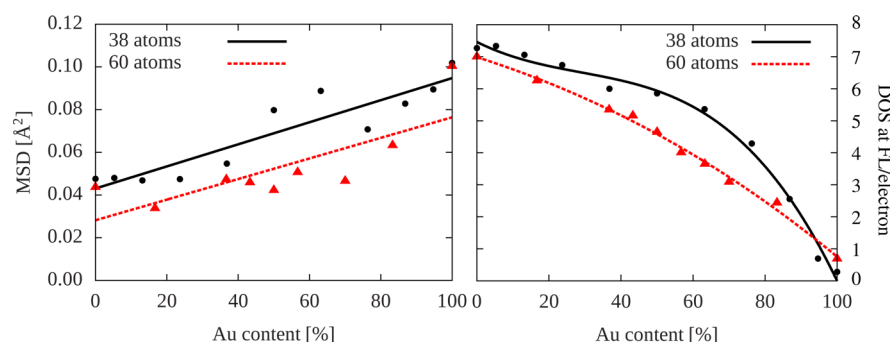
Figure 6. Left: MSD and linear fit to the MSD of 38-atom (black triangles) and 60-atom (red triangles) clusters. Right: Density of states at the Fermi level for 38-atom and 60-atom clusters and the corresponding cubic polynomial fits.

■ APPENDIX

Statistical uncertainties in the MSD of the 60-atom NP and, because of its small size, also in the 38-atom NP must be taken into account when constructing a volcano-like plot by multiplying the DOS at the Fermi level and the MSD. We therefore used a polynomial least-squares method to fit the data for the MSD and the DOS at the Fermi level. The latter was fitted by a cubic polynomial. For the former we used a linear fit as a rather simplistic model for the trend of an increasing MSD with increasing Au content. Figure 6 shows the MSD (left), the DOS at the Fermi level (right), and the corresponding fit functions. For the visualization of the volcano plot in Figure 5 the DOS at the Fermi level for NP with 100% Au content and the MSD for NP with 0% Au content, respectively, were shifted to zero. For the 38-atom particle the corresponding shifts were 0.28 (units as discussed below) and 0.05 $Å^2$ and for the 60-atom particle 0.70 and 0.04 $Å^2$, respectively. The units for the DOS were obtained in the following way: The Kohn−Sham DOS was folded with a Gaussian of width of 0.08 eV, normalized to the number of valence electrons, and integrated from the HOMO eigenvalue to 1 eV below the HOMO eigenvalue. The given values (0.28 and 0.70) refer to the thus-obtained units.

■ AUTHOR INFORMATION

Corresponding Author
*E-mail: stephan.kuemmel@uni-bayreuth.de.
Notes
The authors declare no competing financial interest.

■ ACKNOWLEDGMENTS

■ REFERENCES

(1) Haruta, M.; Kobayashi, T.; Sano, H.; Yamada, N. Novel Gold Catalysts for the Oxidation of Carbon Monoxide at a Temperature Far Below 0 °C. *Chem. Lett.* **1987**, *16*, 405−408.

(2) Sanchez, A.; Abbet, S.; Heiz, U.; Schneider, W.-D.; Häkkinen, H.; Barnett, R. N.; Landman, U. When Gold Is Not Noble: Nanoscale Gold Catalysts. *J. Phys. Chem. A* **1999**, *103*, 9573−9578.

(3) Tian, N.; Zhou, Z.-Y.; Sun, S.-G.; Ding, Y.; Wang, Z. L. Synthesis of Tetrahexahedral Platinum Nanocrystals with High-Index Facets and High Electro-Oxidation Activity. *Science* **2007**, *316*, 732−735.

(4) Herzing, A. A.; Kiely, C. J.; Carley, A. F.; Landon, P.; Hutchings, G. J. Identification of Active Gold Nanoclusters on Iron Oxide Supports for CO Oxidation. *Science* **2008**, *321*, 1331−1335.

(5) Schrinner, M.; Ballauff, M.; Talmon, Y.; Kauffmann, Y.; Thun, J.; Möller, M.; Breu, J. Single Nanocrystals of Platinum Prepared by Partial Dissolution of Au-Pt Nanoalloys. *Science* **2009**, *323*, 617−620.

(6) Zeng, J.; Zhang, Q.; Chen, J.; Xia, Y. A Comparison Study of the Catalytic Properties of Au-Based Nanocages, Nanoboxes, and Nanoparticles. *Nano Lett.* **2010**, *10*, 30−35.

(7) Walsh, M. J.; Yoshida, K.; Kuwabara, A.; Pay, M. L.; Gai, P. L.; Boyes, E. D. On the Structural Origin of the Catalytic Properties of Inherently Strained Ultrasmall Decahedral Gold Nanoparticles. *Nano Lett.* **2012**, *12*, 2027−2031.

(8) Ferrando, R.; Jellinek, J.; Johnston, R. L. Nanoalloys: From Theory to Applications of Alloy Clusters and Nanoparticles. *Chem. Rev.* **2008**, *108*, 845−910.

(9) (a) Lou, Y.; Maye, M. M.; Han, L.; Luo, J.; Zhong, C.-J. Gold-Platinum Alloy Nanoparticle Assembly As Catalyst for Methanol Electrooxidation. *Chem. Commun.* **2001**, *2001*, 473−474. (b) Luo, J.; Njoki, P. N.; Lin, Y.; Mott, D.; Wang, L.; Zhong, C.-J. Characterization of Carbon-Supported AuPt Nanoparticles for Electrocatalytic Methanol Oxidation Reaction. *Langmuir* **2006**, *22*, 2892−2898. (c) Mott, D.; Luo, J.; Njoki, P.; Lin, Y.; Wang, L.; Zhong, C. Synergistic Activity of Gold-Platinum Alloy Nanoparticle Catalysts. *Catal. Today* **2007**, *122*, 378−385. (d) Yang, L.; Shan, S.; Loukrakpam, R.; Petkov, V.; Ren, Y.; Wanjala, B. N.; Engelhard, M. H.; Luo, J.; Yin, J.; Chen, Y.; et al. Role of Support-Nanoalloy Interactions in the Atomic-Scale Structural and Chemical Ordering for Tuning Catalytic Sites. *J. Am. Chem. Soc.* **2012**, *134*, 15048−15060.

(10) Hernandez-Fernandez, P.; Rojas, S.; Ocon, P.; Gomez de la Fuente, J.; San Fabian, J.; Sanza, J.; Pena, M.; Garcia-Garcia, F.; Terreros, P.; Fierro, J. Influence of the Preparation Route of Bimetallic Pt-Au Nanoparticle Electrocatalysts for the Oxygen Reduction Reaction. *J. Phys. Chem. C* **2007**, *111*, 2913−2923.

(11) Zhang, J.; Ma, H.; Zhang, D.; Liu, P.; Tian, F.; Ding, Y. Electrocatalytic Activity of Bimetallic Platinum-Gold Catalysts Fabricated Based on Nanoporous Gold. *Phys. Chem. Chem. Phys.* **2008**, *10*, 3250−3255.

(12) Selvarani, G.; Selvaganesh, S. V.; Krishnamurthy, S.; Kiruthika, G. V. M; Sridhar, P.; Pitchumani, S.; Shukla, A. K. A Methanol-Tolerant Carbon-Supported Pt-Au Alloy Cathode Catalyst for Direct Methanol Fuel Cells and Its Evaluation by DFT. *J. Phys. Chem. C* **2009**, *113*, 7461−7468.

(13) Du, B.; Zaluzhna, O.; Tong, Y. J. Electrocatalytic Properties of Au@Pt Nanoparticles: Effects of Pt Shell Packing Density and Au Core Size. *Phys. Chem. Chem. Phys.* **2011**, *13*, 11568−11574.

(14) Kuai, L.; Geng, B.; Wang, S.; Sang, Y. A General and High-Yield Galvanic Displacement Approach to Au-M (M = Au, Pd, and Pt) Core-Shell Nanostructures with Porous Shells and Enhanced Electrocatalytic Performances. *Chem.—Eur. J.* **2012**, *18*, 9423−9429.

(15) Ilayaraja, N.; Prabu, N.; Lakshminarasimhan, N.; Murugan, P.; Jeyakumar, D. Au-Pt Graded Nano-Alloy Formation and Its

Manifestation in Small Organics Oxidation Reaction. *J. Mater. Chem. A* **2013**, *1*, 4048−4056.

(16) Mihut, C.; Descorme, C.; Duprez, D.; Amiridis, M. D. Kinetic and Spectroscopic Characterization of Cluster-Derived Supported Pt-Au Catalysts. *J. Catal.* **2002**, *212*, 125−135.

(17) Schrinner, M.; Proch, S.; Mei, Y.; Kempe, R.; Miyajima, N.; Ballauff, M. Stable Bimetallic Gold-Platinum Nanoparticles Immobilized on Spherical Polyelectrolyte Brushes: Synthesis, Characterization, and Application for the Oxidation of Alcohols. *Adv. Mater.* **2008**, *20*, 1928−1933.

(18) Peng, Z.; Yang, H. PtAu Bimetallic Heteronanostructures Made by Post-Synthesis Modification of Pt-on-Au Nanoparticles. *Nano Res.* **2009**, *2*, 406−415.

(19) Yancey, D. F.; Carino, E. V.; Crooks, R. M. Electrochemical Synthesis and Electrocatalytic Properties of Au@Pt Dendrimer-Encapsulated Nanoparticles. *J. Am. Chem. Soc.* **2010**, *132*, 10988−10989.

(20) Shao, M.; Peles, A.; Shoemaker, K.; Gummalla, M.; Njoki, P. N.; Luo, J.; Zhong, C.-J. Enhanced Oxygen Reduction Activity of Platinum Monolayer on Gold Nanoparticles. *J. Phys. Chem. Lett.* **2011**, *2*, 67−72.

(21) Norskov, J. K.; Bligaard, T.; Rossmeisl, J.; Christensen, C. H. Towards the Computational Design of Solid Catalysts. *Nat. Chem.* **2009**, *1*, 37−46.

(22) Gaspari, R.; Pignedoli, C.; Fasel, R.; Treier, M.; Passerone, D. Atomistic Insight Into the Adsorption Site Selectivity of Stepped Au(111) Surfaces. *Phys. Rev. B* **2010**, *82*, 041408(R)(1−4).

(23) Hermannsdörfer, J.; Friedrich, M.; Miyajima, N.; Albuquerque, R. Q.; Kümmel, S.; Kempe, R. Ni/Pd@MIL-101: Synergistic Catalysis with Cavity-Conform Ni/Pd Nanoparticles. *Ang. Chem., Int. Ed.* **2012**, *51*, 11473−11477.

(24) Perdew, J. P.; Burke, K.; Ernzerhof, M. Generalized Gradient Approximation Made Simple. *Phys. Rev. Lett.* **1996**, *77*, 3865−3868.

(25) *Turbomole V6.0.*, 2009.

(26) Leppert, L.; Kümmel, S. The Electronic Structure of Gold-Platinum Nanoparticles: Collecting Clues for Why They Are Special. *J. Phys. Chem. C* **2011**, *115*, 6694−6702.

(27) (a) Körzdörfer, T.; Kümmel, S.; Marom, N.; Kronik, L. When To Trust Photoelectron Spectra From Kohn-Sham Eigenvalues: The Case of Organic Semiconductors. *Phys. Rev. B* **2009**, *79*, 201205(R)(1−4). (b) Körzdörfer, T.; Kümmel, S.; Marom, N.; Kronik, L. *Phys. Rev. B* **2010**, *82*, 129903(E).

(28) Dauth, M.; Körzdörfer, T.; Kümmel, S.; Ziroff, J.; Wiessner, M.; Schöll, A.; Reinert, F.; Arita, M.; Shimada, K. Orbital Density Reconstruction for Molecules. *Phys. Rev. Lett.* **2011**, *107*, 193002(1−5).

(29) Logsdail, A.; Paz-Borbón, L. O.; Johnston, R. L. Structures and Stabilities of Platinum-Gold Nanoclusters. *J. Comput. Theor. Nanosci.* **2009**, *6*, 857−866.

(30) Sheppard, D.; Terrell, R.; Henkelman, G. Optimization Methods for Finding Minimum Energy Paths. *J. Chem. Phys.* **2008**, *128*, 134106(1−10).

(31) Kresse, G.; Furthmüller, J. Efficient Iterative Schemes for Ab Initio Total-Energy Calculations Using a Plane-Wave Basis Set. *Phys. Rev. B* **1996**, *54*, 11169−11186.

(32) Blöchl, P. E. Projector Augmented Wave Method. *Phys. Rev. B* **1994**, *50*, 17953−17979.

(33) Beret, E. C.; Ghiringhelli, L. M.; Scheffler, M. Free Gold Clusters: Beyond the Static, Monostructure Description. *Faraday Discuss.* **2011**, *152*, 153−167.

(34) Smith, W.; Forester, T. R. DL_POLY_2.0: A General-Purpose Parallel Molecular Dynamics Simulation Package. *J. Mol. Graph.* **1996**, *14*, 136−141.

(35) Leppert, L.; Albuquerque, R. Q.; Kümmel, S. Gold-Platinum Alloys and Vegard's Law on the Nanoscale. *Phys. Rev. B* **2012**, *86*, 241403(R)(1−5).

(36) Sankaranarayanan, S. K. R. S.; Bhethanabotla, V. R.; Joseph, B. Molecular Dynamics Simulation Study of the Melting of Pd-Pt Nanoclusters. *Phys. Rev. B* **2005**, *71*, 195415(1−15).

(37) Mejia-Rosales, S. J.; Fernandez-Navarro, C.; Perez-Tijerina, E.; Montejano-Carrizales, J. M.; Jose-Yacaman, M. Two-Stage Melting of Au-Pd Nanoparticles. *J. Phys. Chem. B* **2006**, *110*, 12884−12889.

(38) (a) Yang, Z.; Yang, X.; Xu, Z. Molecular Dynamics Simulation of the Melting Behavior of Pt-Au Nanoparticles with Core-Shell Structure. *J. Phys. Chem. C* **2008**, *112*, 4937−4947. (b) Yang, Z.; Yang, X.; Xu, Z.; Liu, S. Structural Evolution of Pt-Au Nanoalloys During Heating Process: Comparison of Random and Core-Shell Orderings. *Phys. Chem. Chem. Phys.* **2009**, *11*, 6249−6255.

(39) Sutton, A. P.; Chen, J. Long-Range Finnis-Sinclair Potential. *Philos. Mag. Lett.* **1990**, *61*, 139−146.

(40) Liu, H. B.; Pal, U.; Ascencio, J. A. Thermodynamic Stability and Melting Mechanism of Bimetallic Au-Pt Nanoparticles. *J. Phys. Chem. B* **2008**, *112*, 19173−19177.

(41) Akbarzadeh, H.; Parsafar, G. A. A Molecular-Dynamics Study of Thermal and Physical Properties of Platinum Nanoclusters. *Fluid Phase Equilib.* **2009**, *280*, 16−21.

(42) Hammer, B.; Norskov, J. K. Why Gold Is the Noblest of All Metals. *Nature* **1995**, *376*, 238−240.

(43) Hammer, B.; Norskov, J. K. Electronic Factors Determining the Reactivity of Metal Surfaces. *Surf. Sci.* **1995**, *343*, 211−220.

(44) Piotrowski, M. J.; Piquini, P. C.; Da Silva, J. Platinum-Based Nanoalloys PtTM (TM = Co, Rh, Au): A Density Functional Theory Investigation. *J. Phys. Chem. C* **2012**, *116*, 18432−18439.

(45) Roudgar, A.; Groß, A. Local Reactivity of Metal Overlayers: Density Functional Theory Calculations of Pd on Au. *Phys. Rev. B* **2003**, *67*, 033409(1−4).

(46) Häkkinen, H.; Abbet, S.; Sanchez, A.; Heiz, U.; Landman, U. Structural, Electronic, and Impurity-Doping Effects in Nanoscale Chemistry: Supported Gold Nanoclusters. *Angew. Chem. Int. Ed.* **2003**, *42*, 1297−1300.

(47) Wunder, S.; Lu, Y.; Albrecht, M.; Ballauff, M. Catalytic Activity of Faceted Gold Nanoparticles Studied by a Model Reaction: Evidence for Substrate-Induced Surface Restructuring. *ACS Catal.* **2011**, *1*, 908−916.

(48) Kaiser, J.; Leppert, L.; Welz, H.; Polzer, F.; Wunder, S.; Wanderka, N.; Albrecht, M.; Lunkenbein, T.; Breu, J.; Kümmel, S.; et al. Catalytic Activity of Nanoalloys From Gold and Palladium. *Phys. Chem. Chem. Phys.* **2012**, *14*, 6487−6495.

(49) Pedersen, M. O.; Helveg, S.; Ruban, A.; Stensgaard, I.; Besenbacher, F. How a Gold Substrate can Increase the Reactivity of a Pt Overlayer. *Surf. Sci.* **1999**, *426*, 395−409.

(50) Chen, W.; Schmidt, D.; Schneider, W. F.; Wolverton, C. Ordering and Oxygen Adsorption in AuPt/Pt(111) Surface Alloys. *J. Phys. Chem. C* **2011**, *115*, 17915−17924.

(51) We evaluated the MSD as described in this article for different temperatures between 100 and 500 K for the Au-shell/Pt-core NP with 201 atoms.

(52) Sabatier, P. Hydrogenations et Deshydrogenations par Catalyse. *Ber. Dtsch. Chem. Ges.* **1911**, *44*, 1984−2001.